

Determinations of temperature and density for solar-like Stars using Si XI soft X-ray emission lines

G. Y. Liang, G. Zhao

*National Astronomical Observatories, Chinese Academy of Sciences,
Beijing 100012, P. R. China*

gzhao@bao.ac.cn

ABSTRACT

We study temperature and density sensitivities of ratios of Si XI soft X-ray emission lines, in the wavelength range of 43–54Å. The typical temperature of the formation of the analyzed lines is around 1.6 MK, which makes this analysis complementary to the analysis of He-like triplets being sensitive to hotter plasma. We present theoretical calculations and compare them with ratios obtained from high-resolution X-ray spectra of five solar-like stars: Procyon, α Cen A&B, ϵ Eri, and Capella. We find that our results are in good agreement with results obtained by other authors through different diagnostics, namely the analysis of density- and temperature-sensitive He-like triplet lines. We further estimate the coronal pressure and filling factors from Si XI lines in this study.

Subject headings: atomic data – techniques: spectroscopic – stars : coronae – stars: late-type – X-rays : stars

1. Introduction

Determinations of elemental abundances and structures in a various of stars belong to the most important tasks of observational astronomy and the understanding of the evolution of chemical elements. The temperature structure of emitting layers such as the stellar coronae must be known before elemental abundances can be determined. The density is another important physical parameter to describe the magnetically confined plasma in outer atmospheres of late-type stars, which can be used to estimate the spatial information for the stellar coronae. For those pre-main sequence stars, the constrained density can give us clues for the origin of the X-ray production such as magnetics alike the stellar coronae or a shock due to accretion processes.

Before the launch of missions with high resolution spectrograph such as the *Chandra* and *XMM-Newton*, a determination of the electron temperature of X-ray emitting layers usually adopts a technique of global-fitting to spectra. The determined temperature structure from this technique strongly depends on the determination of continuum level of the observed spectra. The measurement of electron density is not possible for non-solar stars with previous X-ray satellites such as ASCA and ROSAT configured with low- and medium-resolution spectrographs. The observation data provided by high-resolution spectrograph on board new generation satellites *Chandra* and *XMM-Newton*, allow us to estimate this parameter. Individual emission lines can be resolved from high-quality spectra, further the electron temperature can be derived from line intensity ratios such as G value (between intercombination i and forbidden f lines *vs* resonance line r) of He-like ions which was described by Porquet et al. (2001) in detail. Since then, the estimation of the electron density becomes possible from X-ray emission line ratios such as R value between i and f lines He-like ions. Using observation data with lower spectral resolution, n_e and emission measures EM can not be obtained independently, such that no emitting volumes V could be estimated from the relation of $EM = n_e^2 V$. The structural information of the outmost atmosphere of stars was accessible from the analysis of lightcurves for a few special systems such as rotational modulation, eclipse mapping, etc. However, the solution of the reconstructed differential EM is always nonunique, and involves the difficulty of disentangling time-dependent versus geometric variability (Schmitt et al. 1996; Schmitt & Favata 1999; Güdel 2004). Since the operation of the two satellites with high-resolution and high-collecting areas, the two parameters have been derived from spectroscopic methods for every class of X-ray sources by many observers (Brinkman et al. 2000; Canizares et al. 2000; Kastner et al. 2002; Ness et al. 2002, 2003; Raassen et al. 2003; Stelzer & Schmitt 2004; Schmitt et al. 2005, etc.). Using He-like triplet lines, a systematic investigation of the electron temperature and density for late-type stars with various levels of activity, has been made by Ness et al. (2002, 2004) and Testa et al. (2004). However, the UV field significantly affects the He-like triplet lines. Recently, Ness & Schmitt (2005) presented a density diagnostic ratio being independent from the UV field, that therefore allows to disentangle n_e and UV field that both affect the O VII triplet lines. Additionally, the derived density has also been used to estimate the production mechanism (alike stellar corona or accretion) of the X-ray emission in pre-main sequence stars (Stelzer & Schmitt 2004; Schmitt et al. 2005).

Soft X-ray emissions of L-shell ions of silicon have been detected extensively in spectra of stellar coronae. These emissions carried out information of the two physical parameters for the solar-like coronae. In our previous work, we investigated the emission lines of Si X, and diagnosed the coronal electron density using them for late-type star—Procyon (Liang et al. 2006a,b). The soft X-ray emissions arising from 3d—2p, 3s—2p and 3p—2s transitions

of Si XI have also been detected obviously for some cool stars, such as Procyon and α Cen A&B (Raassen et al. 2002, 2003). And the temperature (1.6 MK) of maximum formation of Si XI ion in the ionization equilibrium (Mazzotta et al. 1998), is the typical temperature of corona of stars with low activities, which makes the analysis of Si XI soft X-ray emission lines interesting.

EUV features arising from $2s^2$ – $2s2p$ and $2s^2$ – $2p^2$ transitions of Si XI have been used to derive the electron temperature and density for solar flares. Keenan et al. (1995) presented seven line ratios whereas these ratios are usually sensitive to both the electron temperature and density of the emitting plasma. Moreover measured ratios obtained with the Naval Research Laboratory’s S082A spectrograph on board *Skylab*, are larger than theoretical high-temperature and high-density limits (Keenan et al. 1995). Later, Lang et al. (2001) calculated these line ratios again and compared with solar observations obtained with normal incidence spectrometer on board SOHO CDS, as well as laboratory measurements performed by König et al. (1996). In contrast to the EUV lines, there has been little work on the soft X-ray transitions of Si XI in astrophysical literatures, probably as a result of the limited availability of high quality spectra of stellar in this wavelength region.

This paper is organized as following, we firstly investigate the Si XI soft X-ray emission lines and present theoretical calculations of temperature- and/or density-sensitive line intensity ratios in Sect. 2. A brief description of observations and extractions of line fluxes is presented in Sect. 3. Results and discussions are outlined in Sect. 4. Our conclusions are given in Sect. 5.

2. Theoretical line intensity ratios

Our model of Si XI consists of energetically lowest 350 fine-structure energy levels belonging to configurations $2s^2$, $2s2p$, $2p^2$, $2l3l'$, $2l4l'$, $2l5l'$, $2l6l'$ and $2l7l'$ ($l=s, p$; $l' = 0, 1, \dots, n-1$). Some energy levels are replaced by available experimental values from the NIST database¹ and results of Coutinho & Trigueiros (2001). The theoretical calculation is performed using a fully relativistic method—flexible atomic code (FAC) developed by Gu (2003, 2004). Self-consistent results of electron impact excitation, de-excitation rates and Einstein A -coefficient (including electric- and magnetic-dipole, as well as quadrupole transitions) among the 350 levels were also included in present model. The input atomic data of our model significantly differs from that of CHIANTI code, in which only 46 low-lying energy levels, and the excitation and radiative decay among the 46 levels were included. Present

¹http://physics.nist.gov/cgi-bin/AtData/main_asd

model is an extensive one, and cascade effects on the upper levels of interested transition lines from higher excited levels up to $n = 7$ (n is the main quantum number), have been considered. In our recent work (Liang et al. 2006c), a detailed assessment for the calculated data is performed, which reveals that the atomic data is reliable for diagnostic application. Here, a brief comparison of our data with the input atomic data of CHIANTI code is made as shown in Fig. 1. The top panel of Fig. 1 illustrates the comparison of different theoretical predictions of energy levels with the available experimental ones (the NIST data and that of Coutinho & Trigueiros (2001)). This panel indicates that our energy levels agree with the experimental values within 0.7%, which is better than the theoretical data in the CHIANTI database. NIST only lists the energy levels being less 20 *Ryd*. For higher energy levels of above ~ 20 *Ryd*, Coutinho & Trigueiros (2001) reported some values and determined the energy levels from observed wavelengths by an interactive optimization procedure using the program ELCALC (Radziemski & Kaufman 1969). Comparing with their energy levels also can benchmark our prediction in a certain extent. A better agreement is shown by the filled circles in the upper panel of Fig. 1. The comparison of weighted oscillator strengths is illustrated in the middle panel of Fig. 1, which reveals the two different data is comparable within 20% for most strong transitions ($gf > 0.1$). For those transitions involved in below interested ratios (filled up-triangle in Fig. 1), the two different predictions show a good agreement within 20%. The prominent 3d–2p transitions exhibit a better agreement. For some weak transitions ($gf < 0.1$), large discrepancies up to several factors appear. We suggest such differences are due to different inclusions of configuration interaction (CI) in the different data sources. The work of Aggarwal et al. (2005) and Zeng et al. (2005) has revealed that the consideration of an elaborate CI is very necessary, which support our performance of atomic data calculation. For the effective collision strength (Υ) obtained under the Maxwellian distribution, only the data at a temperature of 1.0 MK (the bottom panel of Fig. 1) is compared for concision, because the temperature is the typical coronal temperature of stars with less activity.

Proton impact excitation is important process for population and de-population of the lowest levels with $n = 2$ complexes. Data from Ryans et al. (1998) was employed in present model, in which the close-coupled impact-parameter method was adopted in the calculation.

The theoretical line intensities are obtained by solving steady-state rate equations with optically thin assumptions, as described by Gu (2003) and Behar et al. (2001). Such assumptions are based on the following reasons. Firstly, photon-excitation and de-excitation rates are negligible in comparison with the electron impact excitation rates in stellar corona, tokamak and laser-produced plasmas, so the processes aren’t considered; secondly, the rates of ionization to and recombination from other ionic stages are lower than bound-bound transition rates; finally, emitted photon directly escapes the plasma, does not collide with particles

again. The line intensities are calculated over a wide range of the electron temperature and density. Here, we pay careful attention on five prominent lines of Si XI, as listed in Table 1. The $3s-2p$ line at 52.306\AA is a strong and isolated line in these selected features. A detailed analysis indicates that following emission line intensity ratios of Si XI ion are sensitive to the electron temperature and/or density:

$$\begin{aligned} R_1 &= I(52.306\text{\AA})/I(43.743\text{\AA}), \\ R_2 &= I(52.306\text{\AA})/I(49.207\text{\AA}), \\ R_3 &= I(49.207\text{\AA})/I(46.391\text{\AA}), \\ R_4 &= I(52.306\text{\AA})/I(46.391\text{\AA}), \\ R_5 &= I(43.743\text{\AA})/I(46.391\text{\AA}), \\ R_6 &= I(46.391\text{\AA})/I(46.283\text{\AA}), \end{aligned}$$

and

$$R_7 = I(52.306\text{\AA})/I(46.283\text{\AA}).$$

Therefore they may be useful diagnostic techniques for the electron temperature and density for all kinds of hot plasma.

Fig. 2 plots these ratios as a function of the electron temperature at $n_e=1.0\times 10^9\text{ cm}^{-3}$, and *vs* the electron density at $\log T_e(\text{K})=6.2$ which is the temperature of maximum formation of Si XI (see solid line in the figure). The ratios are given in photon units, and used throughout the paper. The ratio R_1 varies from 1.7 to 0.9 over the temperature range of $\log T_e(\text{K})=6.0-6.4$, and no variation occurs through a large range of density $10^7-10^{12}\text{ cm}^{-3}$, which is the typical condition of astrophysical, tokamak and EBIT plasmas. This indicates the ratio R_1 is a powerful diagnostic technique of the electron temperature for the hot astrophysical and laboratory plasmas. Ratio R_2 exhibits the same behavior as R_1 , yet this ratio shows a less temperature-sensitivity than that of R_1 .

The ratio R_3 appears to be sensitive to the electron density (shown in Fig. 3), simultaneously it displays a certain sensitivity to the electron temperature. For example, increasing $\log T_e(\text{K})$ from 6.2 to 6.4 leads to 8 per cent variation at $n_e=1.0\times 10^9\text{ cm}^{-3}$. The feature at 46.391\AA being correlative to ratios R_3 , R_4 and R_5 has been identified to be 46.410\AA line arising from $2s2p\ ^3P_2 \rightarrow 2s3d\ ^3D_3$ transition of Si XI in work of Raassen et al. (2002). After adjusting by experimental value from the NIST database, a better wavelength 46.401\AA is obtained in present work. We noticed that the emissivity of the line at 46.404\AA is about 10 per cent relative to that of 46.401\AA , whereas the two lines can not be resolved using present available spectrographs. The expected blending of 46.404\AA line is rather smaller than both the theoretical uncertainty and statistical error in the line flux measurement,

however the blending effect was considered in this study. Ratio R_4 is also sensitive to the electron density, but it is insensitive to the electron temperature in the density-sensitive region, as shown in the lower panel of Fig. 2. The variation is less than 4 per cent when $\log T_e(\text{K})$ changes 0.2 dex. This indicates R_4 is a powerful n_e -diagnostic tool for the line formation region. As R_3 , the blending effect in 46.391 Å line has been also considered in the prediction of R_4 . Ratios R_5 – R_7 show obvious n_e and T_e -dependence, as shown by curves of R_5 and R_6 in Fig. 2. For clearness, the curve of R_7 vs T_e is not given, only its dependence on n_e is plotted in Fig. 3. The resolved lines and their blending contributions are listed in Table 1. From above analysis, we distinguish that R_1 and R_4 are powerful T_e and n_e diagnostic method, respectively. Using the properties of Si XI, we can estimate the electron temperature and density in Si XI emitting region for cool stars.

3. Observations and line fluxes

In this work, we re-analyze the spectra of stars including three normal dwarf stars, i.e., α Cen A&B, Procyon and ϵ Eri, and an active binary system Capella. The detailed descriptions and analyses for these stars are available from many literatures (Schmitt et al. 1996; Mewe et al. 2001; Audard et al. 2001; Ness et al. 2001; Raassen et al. 2002, 2003, etc.). Here, we briefly describe the observations and data reductions for these stars. α Cen A and B are firstly resolved from spectral observation with Low Energy Transmission Grating Spectrometer (LETGS) instrument on board *Chandra* observatory, a detailed description about it was given by Raassen et al. (2003). All observations use the LETGS combined with High Resolution Camera (HRC) detector. Reduction of the LETGS datasets adopts CIAO3.2 software with the science threads for LETGS/HRC-S observations. For the extraction of the spectra of α Cen A&B, a similar procedure used by Raassen et al. (2003) is adopted here under the CIAO environment.

Line fluxes are obtained by locally fitting the emission features using multiple overlapping Gaussian profiles, together with a constant value representing background and (pseudo-)continuum emission, which was determined in line-free regions such as (51–52 Å). The positive order spectra was used to derive the line fluxes because some lines such as 52.306 Å of Si XI lie in the gap between chips in the negative spectra. Determinations of the line fluxes of Si XI lines are difficult because a large amount of emissions of highly ionized magnesium, sulfur and argon is also present in this wavelength range of 43–53 Å. Here we choose Procyon as an example to illustrate. At the shorter wavelength wing of Si XI line at 43.743 Å, a weak line of S XII at 43.649 Å appears as illustrated in the left panel of Fig. 4. Two emission lines of S IX at 49.107 Å and 49.324 Å broaden the shoulder of Si XI line at 49.207 Å as

shown in the right panel of Fig. 4. By the best-fitting to the spectra, observed line fluxes are obtained as listed in Table 1 with 1σ statistical error. In this table, labels such as $3a$ and $3b$ in first column denote this line is blended. For Procyon and α Cen A&B, all prominent lines of Si XI have been identified by Raassen et al. (2002, 2003), and line fluxes are consistent with those derived by us within 1σ statistical error. However, for ϵ Eri and Capella, only the line at 49.207 Å is reported in available literatures.

4. Results and Discussions

4.1. Determinations of T_e

Sect. 2 has revealed that R_1 and R_2 are good T_e diagnostic tools. By comparing observed line ratios R_1 and R_2 with the theoretical predictions as shown in Fig. 5, the electron temperature of the Si XI emitting region is obtained, as listed in Table 2. The observed ratio R_1 of α Cen A slightly higher than other observed ratios, and the value is up to 1.72. This implies that the diagnosed temperature is lower than that of other stars. In other cases, the observed ratios of R_1 are ranging from 1.2 to 1.4. In consequence, the diagnosed electron temperatures lie within ~ 1.5 – 2.4 MK. These results are consistent with the temperature (1.6 MK) of maximum formation of Si XI in the ionization equilibrium (Mazzotta et al. 1998). The results also agree with the peak temperature of differential emission measure (DEM) constructed from a global spectral fitting for normal stars including Procyon and α Cen (Raassen et al. 2002, 2003), and low-temperature component of DEM for active binary system—Capella (Audard et al. 2001). For α Cen binary system, our results further confirms Raassen’s conclusion derived from He-like triplet that α Cen B (K1V) component is hotter than the α Cen A (G2V) component (Raassen et al. 2003).

As stated in Sect.2, R_2 shows a less sensitivity than that of R_1 , so measured ratios are compatible with the upper limit of the theoretical prediction within 1σ statistical error. In the case of Procyon, Raassen et al. (2002) have reported that the Si XI line at 49.207 Å is contaminated by Ar IX line at 49.181 Å which can not be resolved out by present LETGS instrument on board *Chandra* observatory. Therefore, the correct extraction of the fraction of Ar IX line is very important. Fortunately, Lepson et al. (2003) also detected this line in their recent experiment conducted in EBIT measurement for L-shell spectra of highly charged argon. Using the experimental ratio (1.11) between the lines at 48.737 Å and 49.181 Å of Ar IX measured in the EBIT facility, we extracted the contribution of Ar IX line and rederived the ratio R_2 . The weak T_e -dependence of the ratio of the two Ar IX lines supports the direct application of the experimental value. Taking Procyon star as an example, the Ar IX line at 48.730 Å has been obviously detected and no other contamination. We conclude that the

Ar IX line at 49.181 \AA occupies about 18 per cent to the total flux around 49.207 \AA . The intensity of the Ar IX line is nearly 2σ errors. By considering the ~ 18 per cent contribution, the ratio R_2 increases from 0.52 ± 0.13 to 0.64 ± 0.14 , accordingly the derived temperature drops from 7.07 to 2.24 MK which shows consistency with that derived from R_1 within error. For our other sample, we measured the line flux of Ar IX around 48.730 \AA , and performed similar procedure as in Procyon. The derived temperatures show an good agreement with those from R_1 within 1σ error. We also notice that the intensity of Ar IX line relative to Si XI lines changes with the coronal temperature, and specifically, a lower contamination from Ar IX lines is expected for more active stars.

4.2. Determinations of n_e

Sect. 2 indicated that R_4 is a powerful diagnostic tool for the electron density in the Si XI emitting region of hot plasma. By comparing the observed ratios with theoretical prediction, we derived the electron density in the Si XI emitting region of coronal plasma, as shown in Fig. 5. Here, the comparison of R_4 together with R_3 is illustrated in Fig. 6. Table 3 lists the observed line ratios with 1σ statistical error and the diagnosed density for our sample.

The first impression of Fig. 6 is the uncertainty of observed line ratios appearing to be large, and almost all the observed ratios of R_4 agreeing with high-density limit in statistical error with exception of α Cen B case being agreement with low-density limit. A long exposure times are necessary to better constrain the density from R_4 . Yet present line ratio measurements still can give us some clues for the Si XI emitting region, that is the lower or upper density limit can be constrained from our measurements. We note that mean value of the electron density for our sample is above $2 \times 10^8 \text{ cm}^{-3}$, which is the typical density of solar quiescent coronal plasma. For the ratio R_3 , the contaminated Si XI line at 49.207 \AA is concerted, so the blending effect due to the Ar IX line is considered as above subsection. Taking Procyon as an example, R_3 drops from 3.60 ± 1.07 to 2.95 ± 0.86 by taking into account the contamination. A density of $< 8.8 \times 10^{10} \text{ cm}^{-3}$ is obtained, which agrees with that constrained by R_4 within 1σ statistical error. Since the large statistical errors, only the lower or upper limit of the density is given for our sample as listed in Table 3.

4.3. Comparison between present and published results

The temperature of maximum formation of Si XI is close to that of N VII emission lines, therefore the physical conditions in Si XI and N VII emitting region can be compatible. For N VII, the temperature can be derived in principle from ratio between $\text{Ly}\alpha$ line and $\text{Ly}\beta$ line. However the $\text{Ly}\beta$ line generally is faint. So the temperature derived from ratio between $\text{Ly}\alpha$ line and resonance line of He-like ion can trace the this information. Firstly, we compare our results of T_e with those derived from emissions of H- and He-like N ions as shown in Table 4. In this table, $\text{Ly}\alpha/r$ column represents temperature derived from ratio between $\text{Ly}\alpha$ and resonance line r of He-like N VI, while the next column represents temperature constrained by ratio between $\text{Ly}\alpha$ and sum of triplet lines of He-like N VI, whereas the last column G denotes the temperature obtained from the ratio $i + f$ vs resonance line. All the earlier results are from work of Ness et al. (2002). Present results are slightly higher than those determined from emissions of H- and He-like N, whereas they agree within 1σ statistical error. The results from G ratio seem to systematically underestimate T_e as reported by Testa et al. (2004).

Secondly, we compare present results of n_e with those available from literatures as shown in Table 5. In available literatures, the density of cooler plasma of stellar coronae are usually derived from the ratio between the intercombination (i) and forbidden (f) lines of He-like carbon, nitrogen and oxygen ions. Above comparison has denoted the temperature of Si XI (or N VII) emitting region is consistent with that of N VI and N VII mixing region. So we presumed the emissions of N VI-VII and Si XI are emitted by the same plasma, that is the density derived from different techniques should be comparable. Table 5 reveals present results agree with the previous work of Ness et al. (2002) from emissions of H- and He-like nitrogen. In the case of α Cen B, the constrained upper limit of density is obviously lower than the density determined by Ness et al. (2002) within 1σ error, however they agree within 2σ error, such deviation can attribute to the low S/N. In the work of Ness et al. (2002), the effect of radiative field has been considered.

4.4. Electron pressure and filling factor

Large errors in ratios of Si XI result in large uncertainties in deduced electron temperatures and densities, which imply large uncertainties in derived electron pressures. Here, we adopt the n_e corresponding to the best-fit value of R_4 to trace the information about the pressures and structures in line forming regions. Evaluating now the coronal pressure ($p = k_B n_e T_e$) for stars studied here as shown in Table 6. For Procyon, present result is similar to that derived from N VI (4.4 dyn/cm^2) by Ness et al. (2001). Argiroffi et al. (2003)

also evaluated the pressure using the derived T_e and n_e from O VII for Capella, and a upper limit of ~ 6.0 dyn/cm² was obtained, which is in good agreement with present result of 5.57 dyn/cm². The electron pressure of ϵ Eri appears higher than other cases by a factor of ~ 2 , and which is also slightly higher than that (6.60 dyn/cm²) derived by Jordan et al. (2001) using UV emission lines of Si III and O IV.

In terms of these deduced n_e and T_e , we further estimate the coronal structure through filling factors in the line forming region. We firstly derive emitting (coronal) volumes V_{cor} according to a formula $EM_{\text{ion}} = 0.85n_e^2V_{\text{cor}}$, whereas EM_{ion} represents a ion-specific emission measure which is determined by the correlation between ion-specific luminosity ($L_{\text{X,ion}}$) and line peak emissivity ($\epsilon_\lambda(T_m)$),

$$EM_{\text{ion}} = \frac{L_{\text{X,ion}}}{\epsilon_\lambda(T_m)}.$$

Here, the cleanest line at 52.306 Å is used to deduce the ion-specific emission measure. For the peak emissivity, two different values from present calculation and the Astrophysical Plasma Emission Code (APEC) database are adopted. Secondly, we estimate available volumes V_{avail} which can potentially be filled with coronal plasma. And an assumption is made to derive V_{avail} , that is the plasma is confined in an uniform distribution of loop structures obeying the loop scaling law of Rosner et al. (1978, hereafter RTV):

$$n_{e,\text{hot}}L = 1.3 \times 10^6 T_{\text{hot}}^2$$

with the electron density $n_{e,\text{hot}}$ and the plasma temperature T_{hot} at the loop top. Güdel et al. (1997) regarded the loop-top temperature as equivalent to the hotter component of a two-temperature distribution, while the temperature of the hotter component has a such relation:

$$T_{\text{hot}}^4 = \frac{L_X}{55} \left(\frac{R_\star}{R_\odot} \right)^{-2}.$$

The density at the loop-top $n_{e,\text{hot}}$ we derive it from the measured density $n_e(\text{Si XI})$ assuming pressure equilibrium in a given loop, i.e., $n_e T_{\text{ion}} = n_{e,\text{hot}} T_{\text{hot}}$. From these considerations, the available volumes V_{avail} can be expressed as

$$V_{\text{avail}} = \frac{4\pi 1.3 \times 10^6 R_\star^{1/2} R_\odot^{3/2}}{n_e T_{\text{ion}}} \left(\frac{L_X}{55} \right)^{3/4}$$

in cgs units. The ratio of these volumes is defined as the filling factor

$$f = \frac{V_{\text{cor}}}{V_{\text{avail}}}.$$

In Table 6, we derive the filling factor for Si XI emitting regions along with the deduced electron pressures. A few percent of the filling factor for stellar surface is derived again from another line ratios. Present peak emissivity ($4.31 \times 10^{-16} \text{phot.cm}^3 \text{s}^{-1}$) is lower than the APEC result ($5.72 \times 10^{-16} \text{phot.cm}^3 \text{s}^{-1}$) by 25%, which straightforward results in the filling factor slightly higher as indicated in Table 6. In our prediction, silicon abundance of the solar photospheric of Güdel et al. (1997) is adopted, and the ionization equilibrium calculation of Mazzotta et al. (1998) is used to deduce the emissivity for Si XI emission lines. The different peak emissivity might be due to the different atomic data performed with the different inclusion of CI. Moreover, cascade effects from higher excited levels has been considered in present prediction.

Ness et al. (2004) also derived the filling factor for a large sample of stellar coronae using O VII and Ne IX lines, and very small filling factor was found again. Assuming balance between radiation losses and the net conductive flux, Sim & Jordan (2003) derived *area* filling factor ranging from the transition to the inner corona for ϵ Eri. The derived temperature from Si XI emission is ~ 2 MK. So the derived filling factors may be comparable with ones from O VII. The comparison illustrated in Table 6 confirms this point. Testa et al. (2004) also investigated filling factors using Mg XI and O VII for 22 active stars. And they concluded that the surface coronal filling factors are $\sim 10^{-4}$ — 10^{-1} and $\sim 10^{-3}$ —1 for the hotter plasma with $T_e \sim 10^7$ K and the cooler plasma with $T_e \sim (2-3) \times 10^6$ K, respectively. Using the derived electron temperature and density from Si XI, filling factor of 10^{-3} to 10^{-2} is estimated from Si XI, which shows an agreement with that derived from O VII by Testa et al. (2004) for active stars.

Since the lower or upper limits of the density are obtained from Si XI for our sample, we further present the real constraints on the pressure and filling factors as shown in Table 7. We estimated the pressure in magnetic loops is larger than $\sim 0.5 \text{ dyn/cm}^2$ for our sample except for Procyon. This result is complementary to the work of Argiroffi et al. (2003), who derived the upper limits from O VII triplets. The filling factors being less than $\sim 4\%$ are estimated, which shows good consistency with results constrained by O VII triplets. For α Cen B, the lower limit of f (0.36%) and upper limit of p (2.75 dyn/cm^2) are estimated.

5. Conclusion

In summary, we investigate L-shell soft X-ray emission lines of Si XI by using a more complete kinetic model. In this model, cascade effect from higher excited levels with $n = 7$ on the upper levels of the present interested lines has been included. Our analysis reveals that some line intensity ratios such as R_1 and R_2 , provide useful temperature diagnostics in

a temperature range of 5.5—6.5 (in $\log T_e(\text{K})$), while R_4 is useful to diagnose the density in a range of $10^{8-10} \text{ cm}^{-3}$.

By comparing the observed ratios with theoretical prediction, the electron temperature and density for our sample including normal stars (Procyon and α Cen A&B) and active binary system—Capella, have been determined. The constrained temperatures by R_1 with 1.6—2.4 MK, are consistent with the temperature of maximum Si XI fractional abundance in the ionization equilibrium (Mazzotta et al. 1998) and the peak temperature of the DEM constructed from a global fitting of spectra for inactive stars. Since the blending effect in R_2 from Ar IX line at 49.181 Å, the correct line flux measurement of 49.207 Å may induce a certain of systematical errors. Using the experimental ratio (1.11) of Ar IX lines between 48.730 Å and 49.181 Å, we re-derived R_2 and the temperatures, yet they show a good agreement with those constrained by R_1 . Taking into account the contamination of Ar IX line, densities constrained by R_3 also show agreement with those by R_4 within 1σ statistical error.

Temperatures determined by Si XI emissions slightly higher than ones constrained by emissions of H- and He-like N, whereas they are in agreement within 1σ error. So we presume the emissions of N VI-VII and Si XI are emitted by the same plasma. The yielded temperatures from G ratio are systematically lower than present ones as reported by Testa et al. (2004). This may be due to the slightly lower peak temperature (1.4 MK) of the contribution function of the N VI triplets. An agreement of the densities from the two different line ratios of highly charged silicon and nitrogen, is found. This further suggests that the Si XI and N VI-VII emitting plasma may be confined in the same loop.

A filling factor of 10^{-3} to 10^{-2} is derived for our sample from Si XI, and a upper limit of 4% is obtained. Such results are consistent with the findings of Testa et al. (2004) and Ness et al. (2004) that filling factors are much smaller than unity; they also support the findings of Testa et al. (2004) that the filling factor of cooler plasma is directly proportional to the X-ray surface flux of stars.

G. Y. thanks Dr. J.-U. Ness, Arizona State University, for his very useful discussion. This work was supported by the National Natural Science Foundation under Grant No. 10433010, 10403007 and 10521001.

REFERENCES

Aggarwal K. M., Keenan F. P., & Nakazaki S., 2005, A&A, 436, 1141

- Argiroffi C., Maggio A., & Peres G., 2003, A&A, 404, 1033
- Audard M., Behar E., Güdel M., et al., 2001, A&A, 365, L329
- Behar E., Cottam J., Kahn S. M., et al., 2001, ApJ, 548, 966
- Brinkman A. C., Gunsing C. J. T., Kaastra J. S., et al., 2000, ApJ, 530, L111
- Canizares C. R., Huenemoerder D. P., Davis D. S., et al., 2000, ApJ, 539, L41
- Coutinho L. H., & Trigueiros A. G., 2001, J. Quant. Spectrosc. Radiat. Transfer, 64, 5
- Gu M. F., 2003, ApJ, 590, 1131
- Gu M. F., 2004, in proceeding of *14th APS Topical Conference on Atomic Processes in Plasmas*, eds. Cohen J. S., Mazevet S. and Kilcrease D. P.
- Güdel M., 2004, The Astron. Astrophys. Rev., 12, 71
- Güdel M., Guinan E. F., & Skinner S. L., 1997, ApJ, 483, 947
- Jordan C., Sim S. A., McMurry A. D., & Aruvel M., 2001, Mon. Not. R. Astron. Soc., 326, 303
- Kastner J.H., Huenemoerder D. P., Schulz N. S., et al. 2002, ApJ, 567, 434
- Keenan F. P., Greer C. J., & Foster V. J., 1995, Solar Physics, 161, 159
- König R., Kolk K.-H., & Kunze H.-J., 1996, Phys. Scripta, 53, 679
- Lang J., Brooks D. H., O'mullane M. G., et al., 2001, Sol. Phys., 201, 37
- Lepson J. K., Beiersdorfer P., Behar E., et al., 2003, ApJ, 590, 604
- Liang G. Y., Zhao G., & Shi J. R., 2006a, Mon. Not. R. Soc., 368, 196
- Liang G.Y., Zhao G., & Shi J. R., 2006b, AJ, <http://arxiv.org/astro-ph/0604188> (in press)
- Liang G. Y., Zhao G., & Zeng J. L., 2006c, At. Data and Nucl. Data Tables, (in referee)
- Mewe R., Raassen A. J. J., Drake J. J., et al., 2001, A&A, 368, 888
- Mazzotta P., Mazzitelli G., Colafrancesco S., & Vittorio N., 1998, ApJS, 133,403
- Ness J. -U., Brickhouse N. S., Drake J. J., & Huenemoerder D. P., 2003, ApJ, 598, 1277

- Ness J. -U., Güdel M., Schmitt J. H. M. M., Audard M., & Telleschi A., 2004, *A&A*, 427, 667
- Ness J. -U., Mewe R., Schmitt J. H. M. M., et al., 2001, *A&A*, 367, 282
- Ness J. -U., Schmitt J. H. M. M., Burwitz V., et al., 2002, *A&A*, 394, 911
- Ness J. -U., & Schmitt J. H. M. M., 2005, *A&A*, 444, L41
- Porquet D., Mewe R., Dubau J., et al., 2001, *A&A*, 376, 1113
- Raassen A. J. J., Mewe R., Audard M., et al., 2002, *A&A*, 389, 228
- Raassen A. J. J., Ness J.-U., Mewe R., et al., 2003, *A&A*, 400, 671
- Radziemski L. J., & Kaufman V., 1969, *J. Opt. Soc. Am.*, 59, 424
- Ryans R. S. I., Foster-Woods V. J., Copeland F., et al., 1998, *At. Data and Nucl. Data Tables*, 70, 179
- Rosner R., Tucker W., Vaiana G. S., 1978, *ApJ*, 220, 643
- Schmitt J. H. M. M., Drake J. J., Haisch B. M., et al., 1996, *ApJ*, 467, 841
- Schmitt J. H. M. M., & Favata F., 1999, *Nature*, 401, 44
- Schmitt J. H. M. M., Robrade J., Ness J. -U., et al., 2005, *A&A*, 432, L35
- Sim S. A., & Jordan C., 2003, *Mon. Not. Astron. Soc.*, 346, 846
- Stelzer B., & Schmitt J. H. M. M., 2004, *A&A*, 418, 687
- Testa P., Drake J. J., & Peres G., 2004, *ApJ*, 617, 508
- Zeng J. L., Liang G. Y., Zhao G., et al., 2005, *Mon. Not. Astron. Soc.*, 357, 440

Table 1. Line fluxes of interested lines for 5 late-type stars, and its identification. The theoretical wavelength is from calculation of FAC (Liang et al. 2006c), which is corrected by available experimental energy levels.

Index	$\lambda_{\text{obs}}(\text{\AA})$	$\lambda_{\text{theo}}(\text{\AA})$	Ion	Transition	Line fluxes (in unit of $\times 10^{-4} \text{phot.cm}^{-2} \text{s}^{-1}$)				
					Procyon	α Cen B	α Cen A	ϵ Eri	Capella
1	43.743	43.757	Si XI	$2s^2 \ ^1S_0 - 2s3p \ ^1P_1$	0.54 ± 0.08	0.35 ± 0.06	0.23 ± 0.05	0.33 ± 0.05	0.61 ± 0.07
2a	46.283	46.294	Si XI	$2s2p \ ^3P_1 - 2s3d \ ^3D_2$	0.25 ± 0.07	0.19 ± 0.05	0.24 ± 0.06	0.15 ± 0.04	0.60 ± 0.08
2b	...	46.260	Si XI	$2s2p \ ^3P_0 - 2s3d \ ^3D_1$...				
2c	...	46.310	Si XI	$2s2p \ ^3P_1 - 2s3d \ ^3D_1$...				
3a	46.391	46.401	Si XI	$2s2p \ ^3P_2 - 2s3d \ ^3D_3$	0.40 ± 0.08	0.19 ± 0.05	0.39 ± 0.07	0.24 ± 0.05	0.43 ± 0.07
3b	...	46.404	Si XI	$2s2p \ ^3P_2 - 2s3d \ ^3D_2$...				
4	48.720	48.730	Ar IX	$2p^5 3s \ ^1P_1 - 2p^6 \ ^1S_0$	0.23 ± 0.06	-	0.14 ± 0.07	0.13 ± 0.04	0.16 ± 0.05
5	49.207	49.229	Si XI	$2s2p \ ^1P_1 - 2s3d \ ^1D_2$	1.44 ± 0.14	0.67 ± 0.07	0.64 ± 0.07	0.71 ± 0.06	1.33 ± 0.09
6	52.306	52.295	Si XI	$2s2p \ ^1P_1 - 2s3s \ ^1S_0$	0.75 ± 0.11	0.43 ± 0.06	0.39 ± 0.07	0.40 ± 0.05	0.73 ± 0.08

Notes: The same label with different lowercase indices (e.g., 3a and 3b) indicates blended line.

Table 2: Diagnosed electron temperature in Si XI emitting region for 5 stars.

Stars	R_1	T_e (MK)	R_2	T_e (MK)
Procyon	1.39 ± 0.41	$1.65^{+1.79}_{-0.80}$	0.64 ± 0.14	$2.24^{+5.82}_{-1.47}$
α Cen B	1.24 ± 0.32	$2.10^{+1.80}_{-0.88}$	0.72 ± 0.20	$1.52^{+5.55}_{-0.85}$
α Cen A	1.72 ± 0.57	< 2.47	0.76 ± 0.24	$1.23^{+4.17}_{-0.69}$
ϵ Eri	1.20 ± 0.33	$2.30^{+2.10}_{-1.01}$	0.62 ± 0.13	$2.76^{+6.53}_{-1.44}$
Capella	1.20 ± 0.27	$2.30^{+1.57}_{-0.87}$	0.67 ± 0.12	$2.02^{+3.03}_{-0.94}$

Table 3: Diagnosed electron density (in unit of $\times 10^9 \text{cm}^{-3}$) in Si XI emitting region for our sample.

Stars	R_3	n_e	R_4	n_e
Procyon	2.95 ± 0.86	< 87.86	1.88 ± 0.65	> 0.03
α Cen B	3.16 ± 0.88	< 5.00	2.26 ± 0.32	< 0.95
α Cen A	2.13 ± 0.82	> 0.52	1.62 ± 0.52	> 0.44
ϵ Eri	2.46 ± 0.73	> 0.25	1.65 ± 0.55	> 0.42
Capella	2.78 ± 0.67	> 0.06	1.71 ± 0.51	> 0.33

Table 4: Present results of temperature and those derived from H- and He-like N ions (Ness et al. 2002). $\text{Ly}\alpha/\text{He}$ represents the flux ratio between the $\text{Ly}\alpha$ line and the sum of triplet lines of N VI.

Stars	Present	T_e (MK)		
		$\text{Ly}\alpha/r$	$\text{Ly}\alpha/\text{He}$	$G = \frac{i+f}{r}$
Procyon	$1.65^{+1.79}_{-0.80}$	1.09 ± 0.13	1.41 ± 0.07	1.28 ± 0.46
α Cen B	$2.10^{+1.80}_{-0.88}$	1.79 ± 0.16	1.43 ± 0.22	< 1.8
α Cen A	< 2.47	1.35 ± 0.09	1.15 ± 0.09	< 1.2
ϵ Eri	$2.30^{+2.10}_{-1.01}$	2.47 ± 0.18	1.95 ± 0.30	< 2.4
Capella	$2.30^{+1.57}_{-0.87}$	2.73 ± 0.08	2.02 ± 0.10	0.46 ± 0.28

Table 5: Present results of electron density and those derived from the ratio between i and f lines of He-like N VI ion (Ness et al. 2002).

Stars	Present	$\log n_e/\text{cm}^{-3}$
		$R = \frac{i+f}{r}$
Procyon	> 7.48	9.96 ± 0.23
α Cen B	< 8.98	9.99 ± 0.65
α Cen A	> 8.64	9.95 ± 0.30
ϵ Eri	> 8.62	10.35 ± 0.33
Capella	> 8.52	9.86 ± 0.12

Table 6: Filling factor and electron pressures p derived from n_e corresponding to the best-fit value of R_4 . For comparison, the filling factor from O VII are also listed (Ness et al. 2004).

Stars	p dyn/cm ²	filling factor f in %		
		Pres.	APEC	O VII
Procyon	2.69	3.78	2.84	1.31
α Cen B	0.70	1.44	1.09	0.62
α Cen A	5.71	0.14	0.10	0.18
ϵ Eri	10.86	0.25	0.19	0.62
Capella	5.57	0.45	0.34	0.64

Table 7: Real constraints on the pressure p (in dyn/cm²) and the filling factor f (in %).

	Procyon	α Cen B	α Cen A	ϵ Eri	Capella
p	> 0.07	< 2.75	> 0.57	> 1.33	> 1.05
f	–	> 0.36	< 1.40	< 2.04	< 3.30

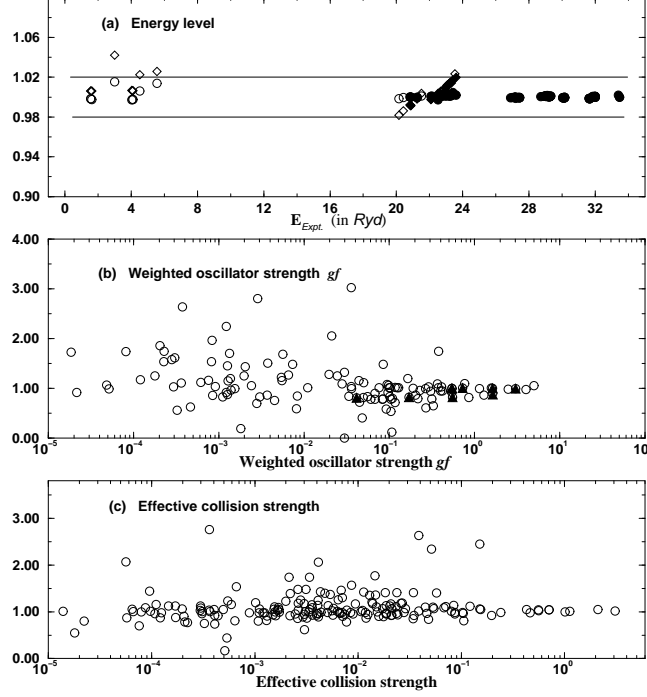


Fig. 1.— Comparison of our calculated atomic data with other available data. (a) Comparison of different theoretical energy levels with available experimental ones (in unit of Ryd). x-axis is the experimental energy from NIST (open symbols) or the results of Coutinho & Trigueiros (2001) (filled symbols), while y-axis represents ratios of different calculation *vs* experimental one. Different symbols correspond to the ratio of results of different calculations *vs* experimental ones. \circ : present results, \diamond : theoretical data in the CHIANTI database. The solid horizontal lines represents 2% uncertainty range. (b, c) Comparison of our results with the input data of CHIANTI code. x-axis is the present result, while y-axis denotes the ratio of the input data of the CHIANTI code *vs* present one. Filled up-triangle denotes the transitions interested in this work.

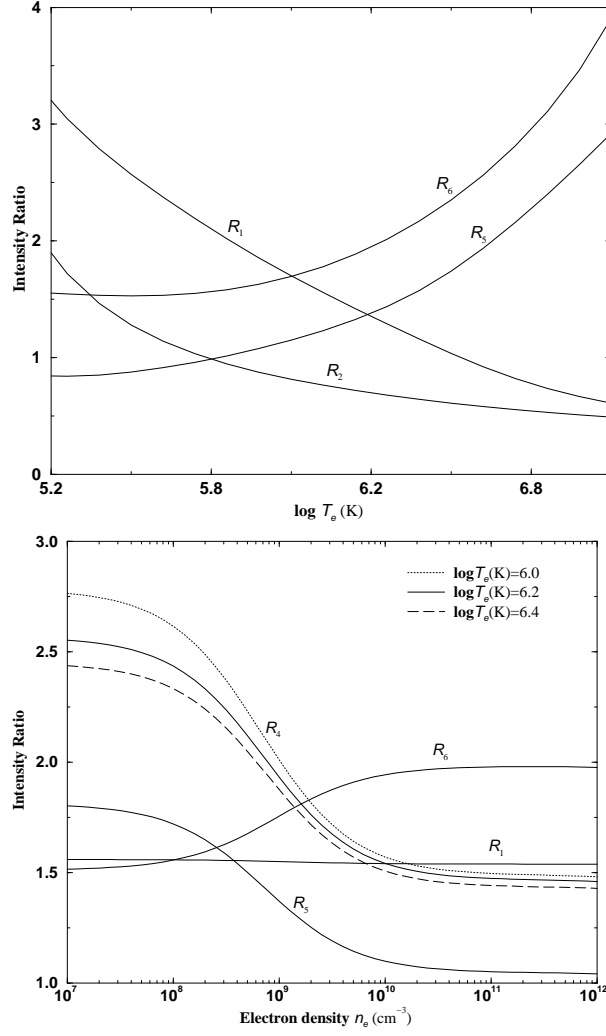


Fig. 2.— The theoretical line ratios of Si XI. *Upper*: plotted as a function of the electron temperature at $n_e=1.0 \times 10^9 \text{ cm}^{-3}$. *Lower*: plotted as a function of the electron density, solid line corresponding to $\log T_e(\text{K})=6.2$.

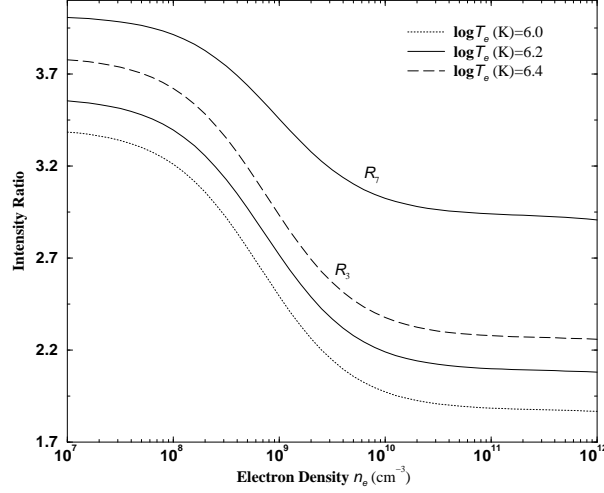


Fig. 3.— The theoretical Si XI emission line ratios *vs* the electron density. The solid line corresponding to $\log T_e (\text{K}) = 6.2$.

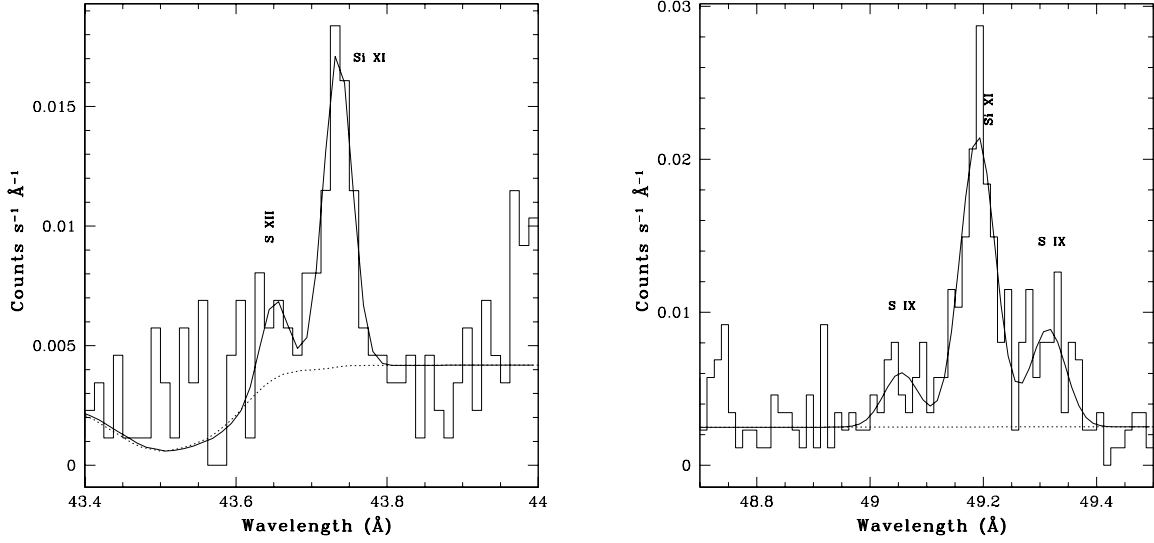


Fig. 4.— Spectrum of Procyon observed with LETGS and best-fit spectra (smooth lines) in wavelength ranges of 43.4–44.0 Å and 48.7–49.5 Å. Dot lines represent the continuum levels. Prominent lines have been labelled above curves.

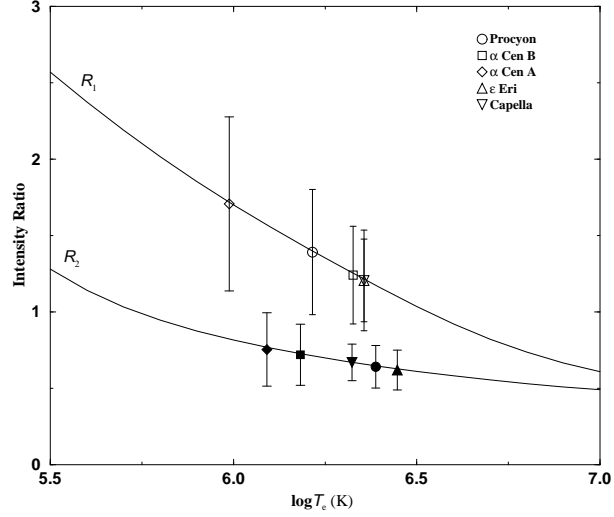


Fig. 5.— Comparison between the theoretical line intensity ratios (R_1 and R_2) and observed ratios of five stars. Opened symbols with error bars are observed values of R_1 , while filled symbols are values of R_2 .

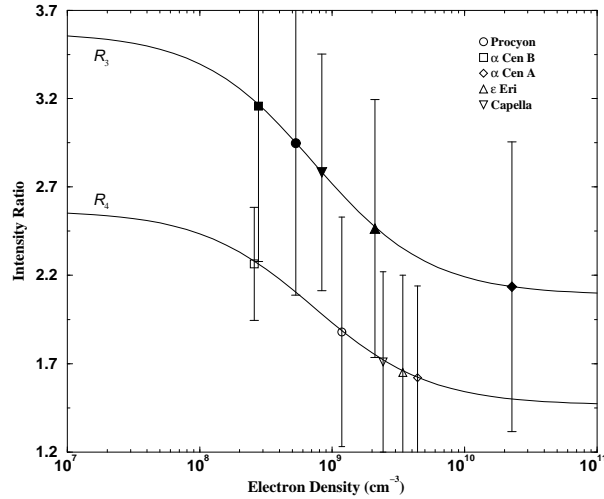


Fig. 6.— Comparison between the theoretical line intensity ratios (R_3 and R_4) and observed ratios of our sample. Opened symbols with error bars represent observed values of R_3 , while filled symbols are for R_4 .